CHEMISTRY OF MATERIALS

pubs.acs.org/cm

Article

InP-Quantum-Dot-in-ZnS-Matrix Solids for Thermal and Air Stability

Seungjin Lee,[†] Laxmi Kishore Sagar,[†] Xiyan Li, Yitong Dong, Bin Chen, Yuan Gao, Dongxin Ma, Larissa Levina, Aidan Grenville, Sjoerd Hoogland, F. Pelayo García de Arquer, and Edward H. Sargent*

Cite This: https://dx.doi.org/10.1021/acs.chemmater.0c02870

Read Online

ACCESS | Metrics & More | Article Recommendations | Supporting Information

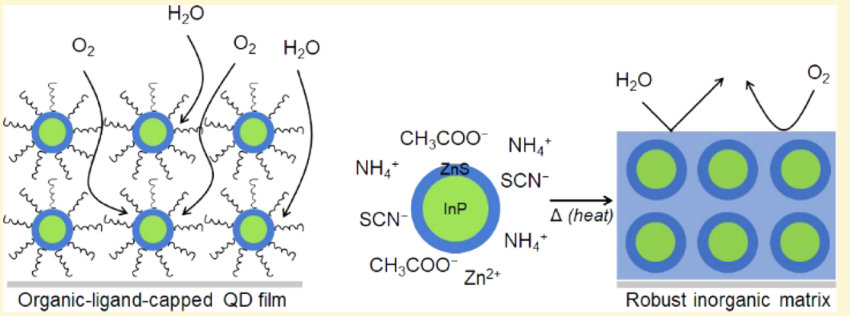

ABSTRACT: InP/ZnS core/shell colloidal quantum dots (QDs) are promising candidates as Cd- and Pb-free emitters owing to their high photoluminescence quantum yield, narrow emission linewidth, and color tunability in the visible range. However, the stability of QD solid films remains an issue: they are vulnerable to oxygen, moisture, and heat. Here, we report the encapsulation of InP/ZnS QDs in a lattice-matched ZnS matrix. We do so by developing a biphasic ligand exchange and uniting it with a sol−gel film assembly. Conventional ZnS precursors, which rely on neutral thiourea, fail to stabilize the QDs in highly polar solvents, leading to their agglomeration prior to matrix formation. Here, we substitute thiourea with ammonium thiocyanate—an ionic compound isomer of thiourea—to stabilize InP/ZnS QDs in a ZnS matrix precursor solution. The stabilized QD and precursor solution is then cast and annealed to trigger the formation of a homogeneous and robust ZnS matrix that protects the QDs. The resulting QD solid films show invariant optical properties following annealing at 200 °C for 1 h under ambient conditions, under continuous laser excitation at 60 mW cm^{-2} for 180 min, and also after a month of storage under ambient conditions. In contrast, the control film exhibits significant degradation of its optical properties after annealing at 200 °C for 1 h, under laser excitation within 20 min, and under ambient conditions within 10 days.

INTRODUCTION

Solution-processed colloidal quantum dots (QDs) have attracted increasing attention for their high photoluminescence quantum yield (PLQY), narrow emission linewidth, and straightforward color tunability depending on the sizes and compositions.[1−3] The performance of Cd-based quantum dot light-emitting diodes (QLEDs) has risen to impressive levels; however, the use of Cd compounds is restricted in certain jurisdictions.[4−7] InP QDs are a promising candidate as Cd-free QDs; InP with a bulk band gap of 1.35 eV (at 300 K) and a large Bohr radius (9.6 nm) is well suited to cover the visible spectrum via controlling the QD size.[6,7]

Developing stable and emissive InP QDs lags behind Cd-based QDs. Many efforts have been devoted to improving the performance of InP QDs for more than 30 years.[5,8] Wide-band-gap semiconductors, such as ZnS, Zn(Ga)S, and ZnSe, epitaxially grown onto InP QDs,[9−13] have been used to confine excitons within InP cores. These approaches enhance the performance of InP QDs, leading to a PLQY of more than 90% in solution.[14,15] Recently, InP QLEDs achieved an external quantum efficiency (EQE) of 6.3% in the green spectrum[16] and 21.4% in the red spectrum.[14]

Despite a significant improvement in the performance of InP QDs, the degradation of the QD films in response to oxygen, moisture, and heat remains an issue.[6,17−21] Oxygen and moisture penetrate easily into the QD film, physically and chemically adsorbing onto QD surfaces and creating trap states.[17,18,22,23]

Encapsulation within a chemically robust matrix is one strategy to avoid degradation of the physicochemical and optoelectronic properties of the QDs. However, the realization of such materials is challenging, as the precursors and formation energy of the most stable matrix often come with poor reactivity on QD surfaces, leading to slow nucleation,

Received: July 9, 2020
Revised: October 17, 2020

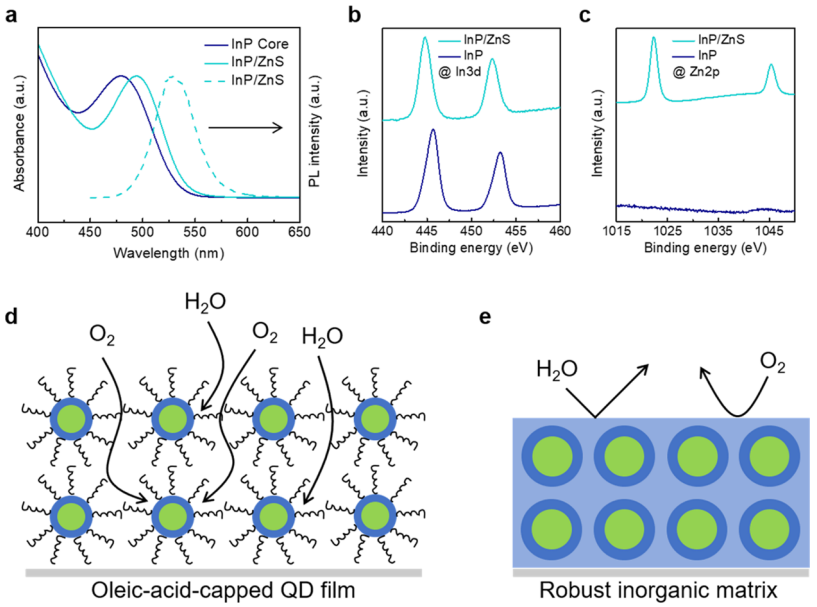

Figure 1. Characterization of the InP core and InP/ZnS core/shell QDs. (a) Absorption spectra of the InP core (navy solid line) and InP/ZnS QDs (cyan solid line) and PL spectrum of InP/ZnS QDs (cyan dashed lines). XPS spectra of (b) In 3d and (c) Zn 2p of the InP core and InP/ZnS QDs. (d) Schematic of the oleic-acid-capped QD film under ambient conditions. (e) Schematic of QDs in a robust inorganic matrix under ambient conditions.

uneven QD incorporation and aggregation, and, ultimately, a lack of stability.[24,25]

Here, we present a strategy to stabilize and protect InP QDs using an inorganic ZnS matrix managing colloidal stability and reactivity between QDs and matrix precursors. We introduce a biphasic ligand exchange using a ZnS sol−gel solution combined with precursor engineering to ensure sufficient matrix seeding on QD surfaces. By replacing a native organic ligand of as-synthesized InP/ZnS QDs with zinc acetate dihydrate ($Zn(CH_3CO_2)_2{\cdot}2H_2O$) and ammonium thiocyanate (NH_4SCN), we transfer QDs to a ZnS precursor solution, in which they form a stable colloid ink. Casting the films from the ink and annealing them at 200 °C result in QDs embedded in the ZnS matrix. Further, we show that QD solid films retain their PLQYs after annealing at 200 °C for 1 h under ambient conditions and additionally after a month of storage under ambient conditions.

EXPERIMENTAL SECTION

Chemicals. Indium (III) acetate ($In(OAc)_3$, 99.99%), Zn-$(CH_3CO_2)_2{\cdot}2H_2O$ (99.999%), NH_4SCN (99.99%), oleic acid (tech. 90%), tris(trimethylsilyl)phosphine ($((TMSi)_3P$, 95%), selenium powder (Se, 99.999%), hexane (reagent grade, >99%), isopropyl alcohol (IPA, anhydrous, 99.8%), toluene-d_8 (99%), and 2-methoxyethanol (99.8%) were purchased from Sigma-Aldrich. Zinc stearate (ZnO, 12.5−14%) and 1-octadecene (ODE, tech. 90%) were purchased from Alfa Aesar. Tri-*n*-octylphosphine (TOP, 97%) and sulfur powder (S, 99%) were purchased from Strem Chemicals. Anhydrous ethanol and *n*-octane were purchased from Caledon. All of the chemicals and solvents above were used without further purification unless stated otherwise. Tris(trimethylsilyl)phosphine is pyrophoric and needs to be stored in an air- and moisture-free environment.

InP Core QD Synthesis. InP QDs were synthesized using a modified approach.[26] In a typical synthesis, 0.100 g (0.34 mmol) of $In(OAc)_3$, 0.282 g (1 mmol) of oleic acid, and 8 mL of ODE were added to a 100 mL Schlenk flask. The reaction mixture was degassed under vacuum at 110 °C for 90 min. The flow was switched to nitrogen, and the flask was cooled to room temperature. Inside a nitrogen-filled glovebox, a phosphorous precursor solution was prepared in a 10 mL vial by adding 1 mL (0.23 mmol) of $(TMSi)_3P$-ODE solution and 1.5 mL of TOP under continuous stirring. The $(TMSi)_3P$ precursor solution was injected into the $In(OAc)_3$ solution at room temperature, and the reaction mixture was heated to 310 °C for 10 min. This process resulted in InP QDs with a first excitonic absorption peak at 475 nm. At the end of the reaction, the temperature was cooled to room temperature. InP QDs were precipitated by adding IPA, centrifuged, and then dispersed in hexane or *n*-octane. To carry out ZnS shell growth, instead of isolating the InP QDs, the temperature was decreased to 200 °C.

InP/ZnS Core/Shell QD Synthesis. InP core QDs with a first excitonic absorption peak at 475 nm were used in InP/ZnS core/shell QD synthesis. For the ZnS shell growth, 6 mL of Zn stearate in ODE and 1.25 mL of TOP-S stock solutions were used. InP core QDs were heated to 200 °C followed by an injection of 1 mL of Zn stearate in ODE. After 5 min, 0.25 mL of TOP-S was added for 5 min. Subsequently, the reaction mixture temperature was heated to 225 °C, and 1 mL of Zn stearate was added slowly for 10 min. TOP-S (0.25 mL) was then added slowly for 5 min. Later, the reaction mixture temperature was increased to 240 °C, and 1 mL of Zn stearate was added for 10 min; then, 0.25 mL of TOP-S was added slowly for 5 min. Finally, the reaction mixture temperature was heated to 270 °C, and 3 mL of Zn stearate along with 0.50 mL of TOP-S was added dropwise over 30 min. The reaction was stopped by cooling the reaction mixture to 45 °C, and the purification of the QDs was carried out under ambient conditions. For the purification of QDs, the reaction mixture was divided into two centrifuge tubes. To each centrifuge tube, 5 mL of IPA, 3 mL of acetone, and 15 mL of ethanol were added, and the tubes were centrifuged at 7000 rpm for 5 min. The QDs were dispersed in 10 mL of hexane and centrifuged at 7000 rpm for an additional 5 min. This step was essential to remove unreacted Zn stearate, which was settled at the bottom. The supernatant was collected and purified one more time by adding 3 mL of IPA, 2 mL of acetone, and 8 mL of ethanol; the mixture was then centrifuged at 7000 rpm for an additional 5 min. Finally, the dots were dispersed in *n*-hexane at a concentration of ~50 mg mL^{-1}.

Ligand Exchange with ZnS Precursor and Growth of the ZnS Matrix on QDs. The ligand exchange was carried out under ambient conditions. Oleic-acid-capped InP/ZnS QDs were dispersed in hexane (10 mg mL^{-1}). The ligand solution was prepared by

https://dx.doi.org/10.1021/acs.chemmater.0c02870
Chem. Mater. XXXX, XXX, XXX−XXX

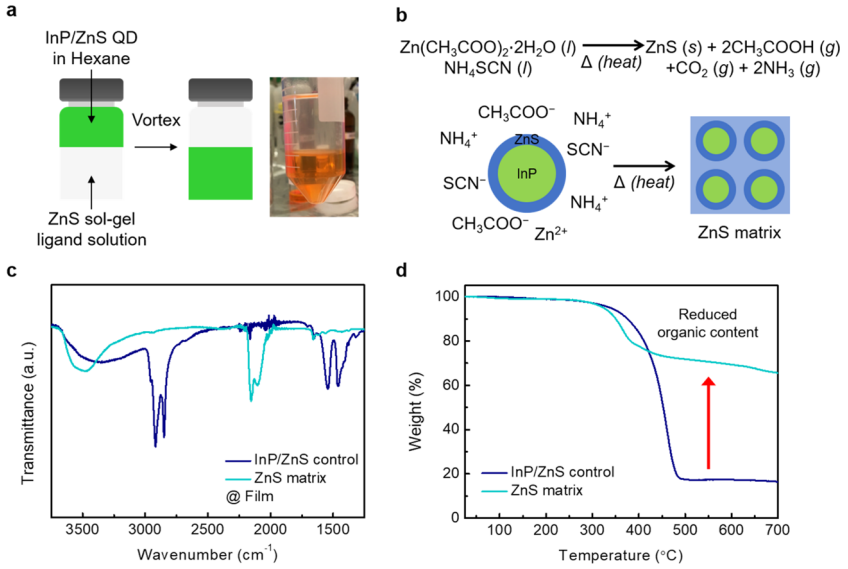

Figure 2. ZnS matrix growth on InP/ZnS QDs (top panel) and their characterization (bottom panel). (a) Schematic and photograph of the biphasic ligand exchange process, demonstrating the transfer of InP/ZnS QDs from hexane to 2-methoxyethanol via ligand exchange. (b) Chemical route and schematic of the growth of the ZnS matrix. Spin-coating the QD ink on a solid-state film and annealing of the film lead to the growth of the ZnS matrix. (c) FTIR spectra and (d) TGA curves of InP/ZnS QDs and QDs in the ZnS matrix.

dissolving $Zn(CH_3CO_2)_2{\cdot}2H_2O$ (0.2 M) and NH_4SCN (0.2 M) in 2-methoxyethanol. The QD solution (5 mL) was added to 5 mL of ligand solution. After vigorous vortexing for 5 min, QDs were transferred to the 2-methoxyethnaol phase via the ligand exchange, and the 2-methoxyethanol phase solution was washed with hexane three times to remove residual oleic acid ligands. Then, the ZnS-precursor-exchanged InP/ZnS QDs were spin-coated on glass substrates at 4000 rpm for 30 s under ambient conditions, followed by annealing them at 200 °C for 1 h.

Precursor Stock Solutions. *$(TMSi)_3P$-ODE Solution.* Commercially available $(TMSi)_3P$ (1.0 g) was diluted in ODE at a concentration of ≈50 mg mL^{-1}.

TOP-S. A saturated TOP-S solution was prepared by mixing and stirring 1.2 g of sulfur powder in 20 mL of TOP inside the glovebox.

Zn Stearate in ODE. Zn stearate (1.0 g) was dispersed in 3 mL of ODE and vortexed for 5 min inside the glovebox.

Absorption Measurements. The optical absorption measurements were performed with a PerkinElmer Lambda 950 UV−vis−NIR spectrophotometer. The solutions were placed in a quartz cuvette with a 1 mm path length. The absorption measurements were performed by dispersing QDs in *n*-octane or hexane. QD films were deposited on glass substrates to measure the solid-state film absorption.

Photoluminescence (PL) and PLQY Measurements. Steady-state and time-resolved PL measurements were performed with a Horiba Fluorolog time-correlated single-photon counting system, equipped with UV−vis−NIR photomultiplier detectors, dual grating spectrometers, and a monochromatized xenon lamp excitation source. The samples were excited at 320 nm using a 500 W xenon lamp. A published method was used to measure PLQYs using an integrating sphere.[26] Light was coupled with the Fluorolog system and the integrating sphere with optical fiber bundles. Time-resolved PL spectra were measured using a 370 nm pulsed laser.

XPS Measurements. XPS spectra were measured using a Thermo Scientific Kα System with an Al Kα source. The films were prepared on glass substrates; there was a 50 eV pass energy and scans were taken at 0.05 eV steps. The atomic ratios were obtained by integrating the area under each peak and scaled by atomic sensitivity factors. We normalized all of the element areas with respect to phosphorous to obtain accurate atomic ratios.

X-ray Diffraction (XRD) Measurements. XRD samples were prepared by drop casting a layer of the desired core or core/shell material from an octane solution on a glass substrate. Measurements were performed on a Rigaku Powder Diffractometer.

Nuclear Magnetic Resonance (NMR) Spectroscopy. ^1H NMR experiments were performed by evaporating the InP/ZnS QD dispersion to dryness under a continuous nitrogen flow and redispersing the obtained QD powder in dry toluene-d_8.

RESULTS AND DISCUSSION

We synthesized InP QD cores by reacting $In(OAc)_3$, oleic acid, and $(TMSi)_3P$ in an ODE solvent.[26] As-synthesized InP QDs have a band edge absorption at 475 nm (Figure 1a). InP QDs have very low PLQY (<1%) due to poor surface passivation and oxidative defects.[5,27] A wider-band-gap ZnS shell is epitaxially grown on InP QDs to improve surface passivation and confinement of electrons and holes in type-I core/shell QDs. Figure 1a shows the absorption and PL spectra of InP/ZnS. After shell growth, the PLQY of InP/ZnS QDs in solution is 50%. Further evidence of shell growth is observed from X-ray photoelectron spectroscopy (XPS): Figure 1b,c shows the XPS spectra of In 3d and Zn 2p for InP and InP/ZnS QDs. Figure S1 shows the ^1H NMR spectra of oleic acid and a well-purified dispersion of as-synthesized InP/ZnS QDs in toluene-d_8. Broadened alkene resonances at 5.4−5.8 ppm and methyl resonances at 1 ppm confirm that InP/ZnS QDs are stabilized by oleate and stearate ligands. Similar observations have been noted for CdSe and PbS QDs.[28] The histogram of the InP/ZnS QD size distribution is shown in Figure S2.

For applications in QD-based optoelectronic devices, QD solutions need to be deposited as a solid-state film. Long organic ligands cannot fully protect QD surfaces from oxygen and water (Figure 1d), leading to degradation of QDs under ambient conditions.[6,17−21] To overcome the vulnerability of QD films to external environments, we propose the growth of an inorganic matrix (Figure 1e). The encapsulation of QDs inside the matrix has the potential to improve the stability of QD films by protecting QDs from oxygen and moisture.

Given that a sol−gel process produces an inorganic solid from precursors, we sought to exchange native organic ligands

https://dx.doi.org/10.1021/acs.chemmater.0c02870
Chem. Mater. XXXX, XXX, XXX−XXX

of as-synthesized InP/ZnS QDs with ZnS sol−gel precursors to encapsulate QDs in a lattice-matched ZnS matrix. We employed a biphasic ligand exchange since ZnS precursors can be dissolved in highly polar solvents, which are not miscible with as-synthesized QD solutions (nonpolar solvents). We used a conventional ZnS precursor solution, which is prepared by dissolving $Zn(CH_3CO_2)_2{\cdot}2H_2O$ and thiourea in 2-methoxyethanol to exchange organic ligands of as-synthesized InP/ZnS QDs. Oleic-acid-capped InP/ZnS QDs dispersed in hexane were transferred to the 2-methoxyethanol phase via ligand exchange; however, the exchanged QDs were not colloidally stabilized in 2-methoxyethanol (Figure S3).

Given that QDs can be colloidally stabilized in the solvent when the QD−solvent interaction is sufficient to overcome the QD−QD attraction, we reasoned that the polar but neutral thiourea cannot provide sufficient interactions with highly polar solvents. We thus sought to use NH_4SCN, which is an ionic compound as well as an isomer of thiourea. We exchanged organic ligands of as-synthesized InP/ZnS QDs with the ZnS precursors ($Zn(CH_3CO_2)_2{\cdot}2H_2O$ and NH_4SCN) through the biphasic ligand exchange process (Figure 2a). Oleic-acid-capped InP/ZnS QDs were transferred to the 2-methoxyethanol phase, forming a stable colloid. The PLQY of the 2-methoxyethaion phase was measured to be 50%, showing that the PLQY of InP/ZnS QDs in solution remains unchanged after ligand exchange. We then deposited the QD ink and annealed the film at 200 °C, resulting in the formation of QDs embedded in the ZnS matrix (see Experimental Section for details).

We then calculated the volume fraction of QDs to the ZnS matrix by observing a variety of absorption after the formation of the ZnS matrix (see detailed measurement methods in Figure S4). The calculated volume fraction of QD to the ZnS matrix is 50%, which entails that electron−hole pairs need to diffuse a ∼modest 5−10 nm to reach QDs. The thickness of QDs embedded in the ZnS matrix can be adjusted by controlling the concentration of ZnS ligand solutions. We measured the thickness of QDs in the ZnS matrix fabricated with different concentrations of ZnS ligand solutions using Dektak measurements (Figure S5). Images of InP/ZnS QDs in the ZnS matrix are shown with and without ultraviolet lamp excitation at 375 nm (Figure S6). Films show bright green emission under UV irradiation.

We performed Fourier transform infrared (FTIR) spectroscopy and found that oleic acid is removed from the QD surface after the ligand exchange process (Figure 2b). The oleic-acid-capped QD film exhibited C−H stretches at 3000−2850 cm^{-1} and C−C and COO^- stretches at 1660−1450 cm^{-1}.[29] C−H, C−C, and COO^- stretches were no longer observed for QDs embedded in the ZnS matrix. Instead, new SCN^- stretches at 2150−2050 cm^{-1} were observed for QDs in ZnS, indicating that SCN^- ligands passivate the surface of QDs.[30]

We carried out thermogravimetric analysis (TGA) to quantify organic contents in the oleic-acid-capped control film and QDs in the ZnS matrix. TGA curves of control films show a significant weight loss of more than 80%, exhibiting decomposition features typical of oleic acid ligands.[6] While remaining thiocyanates start to decompose around 300 °C, QDs in the ZnS matrix show a much lower mass loss compared with the control film, indicating a significant reduction of the organic content.

We carried out high-resolution transmission electron microscopy (HRTEM) to investigate the formation of the ZnS matrix. Control InP/ZnS QDs with diameters ∼4.2 nm are shown in Figure 3a. QDs in the ZnS matrix show crystalline

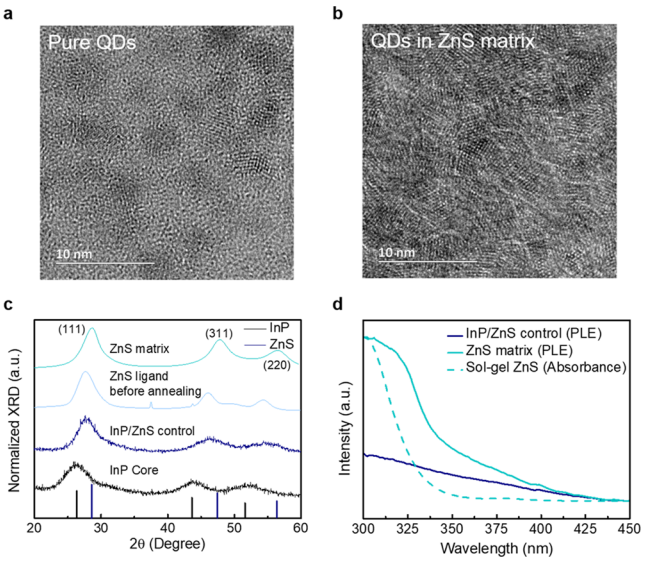

Figure 3. Characterization of ZnS matrix formation on InP QDs. HRTEM images of (a) pure InP/ZnS QDs and (b) QDs in the ZnS matrix. (c) XRD patterns of InP core, InP/ZnS QDs, and InP/ZnS QDs in the ZnS matrix. The black solid line indicates bulk InP, and navy solid lines indicate bulk ZnS XRD patterns. (d) PLE spectra of InP/ZnS QDs (navy solid line) and InP/ZnS QDs in the ZnS matrix (cyan solid line) and absorption spectrum of the sol−gel ZnS film (cyan dashed line).

features in the entire area (Figure 3b), whereas these lattice features were not observed in the space between QDs for the control InP/ZnS QDs. Elemental mapping reveals an even distribution of Zn and S across the area studied for ZnS matrix-embedded QDs (Figure S7).

We further explored the formation of the ZnS matrix by measuring the powder X-ray diffraction (XRD) patterns of InP core QDs, InP/ZnS QDs, and InP/ZnS QDs in the ZnS matrix (Figure 3c). The main peaks of InP at 26.3, 43.6, and 51.6° correspond to the (111), (220), and (311) planes of the zinc blende crystal structure.[31] The three main peaks of ZnS located at 28.5, 47.4, and 56.3° were indexed to the (111), (220), and (311) planes of the zinc blende crystal structure, respectively.[31] After the growth of the ZnS shell on InP QDs, InP/ZnS QDs exhibited a decrease in the full width at half-maximum (FWHM) of XRD peaks, indicating an increase in the crystal size. The XRD peaks of InP/ZnS QDs shifted toward a higher 2θ value, confirming the epitaxial growth of the ZnS shell.[13,32] Unannealed InP/ZnS QDs with ZnS precursor ligands showed similar XRD patterns to control InP/ZnS QDs. In contrast, annealed InP/ZnS QDs showed a further shift of XRD peaks toward higher 2θ values with narrow FWHM of XRD peaks, indicating the formation of the ZnS matrix.

To investigate the possibility of charge transfer from the ZnS matrix to InP QDs, we measured photoluminescence excitation (PLE) spectra of control InP/ZnS QDs and InP/ZnS QDs embedded in the ZnS matrix (Figure 3d). Control InP/ZnS QDs showed a smooth PLE spectrum, whereas the QDs in the ZnS matrix exhibited an abrupt increase of PLE intensity at 335 nm—the absorption edge of the sol−gel ZnS film. The results imply that photogenerated charges or excitons in the ZnS matrix are transferred to InP/ZnS QDs. To confirm

https://dx.doi.org/10.1021/acs.chemmater.0c02870
Chem. Mater. XXXX, XXX, XXX−XXX

efficient carrier transfer from the matrix to QDs, we further studied the excitation wavelength dependence of the PLQY for InP/ZnS QDs in the ZnS matrix. QDs in the ZnS matrix showed similar PLQY values regardless of the excitation wavelength (Figure S8), showing no noticeable decrease of PLQY at excitation of 320 nm, which can excite the ZnS matrix.

We investigated the effect of the ZnS matrix on the optical properties of InP/ZnS QDs by measuring time-resolved and steady-state PL spectra of the InP/ZnS QD film and QDs in the ZnS matrix (Figures 4a and S9). The PL decay was

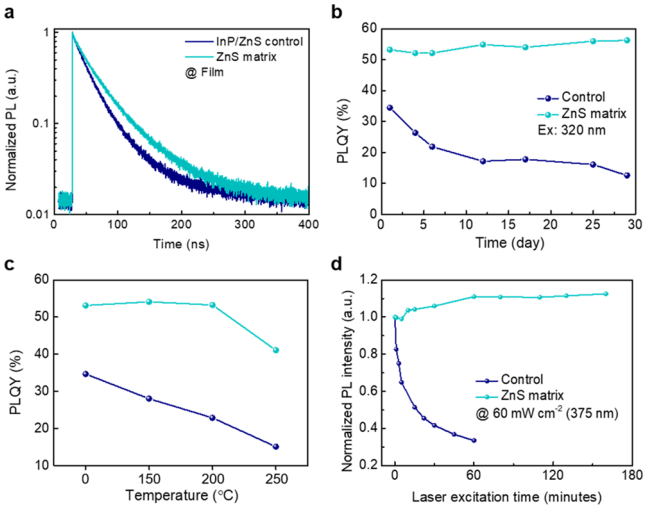

Figure 4. Optical properties and stability tests of InP/ZnS QDs and InP/ZnS QDs in the ZnS matrix solid-state films. (a) Time-resolved PL spectra of InP/ZnS QDs and InP/ZnS QDs in the ZnS matrix, showing enhanced radiative recombination in InP/ZnS QDs in the ZnS matrix compared to InP/ZnS QDs. (b) PLQY stability tests as a function of time for InP/ZnS QDs and InP/ZnS QDs in the ZnS matrix. (c) PLQY stability tests of InP/ZnS QDs and InP/ZnS QDs in the ZnS matrix after annealing at different temperatures for 1 h. (d) Photostability for control InP/ZnS QDs and QDs in the ZnS matrix under continuous 375 nm laser excitation at 60 mW cm^{-2}.

characterized using a biexponential decay function (see detailed parameters in Table S1). Control InP/ZnS QDs showed a higher ratio (0.68) of the fast decay component that involves trap-mediated recombination compared to QDs in the ZnS matrix (0.38). As a result, QDs in the ZnS matrix showed a longer PL lifetime (37.0 ns) with smaller band-tail states in the PL spectrum compared to the control QD film (28.7 ns). We propose that fewer surface traps exist in the QDs in the ZnS matrix as a result of effective passivation of the QD surface. During film deposition, the creation of surface traps in the control QD film may be attributed to the susceptibility of oleic-acid-capped QDs to oxidation.

We investigated the stability of the InP/ZnS QD film vs QDs in the ZnS matrix by measuring PLQY as a function of storage time (Figure 4b). QDs in the ZnS matrix showed a higher initial PLQY (over 50%) than the control film (34%). Additionally, QDs in the ZnS matrix maintained more than 50% of PLQY for a month, indicating that the ZnS matrix protects InP/ZnS QDs. In contrast, the control film exhibited a decrease of less than 20% PLQY within 10 days. We propose that ambient air diffuses into the film and reacts with QD surfaces, producing trap states.

We further tested the effect of the ZnS matrix on the thermal stability of QDs by measuring PLQY after annealing at different temperatures for 1 h, all under ambient conditions (Figure 4c). A decrease of PLQY was observed for the control film at all annealing temperature conditions. As the annealing temperature increases from 150 to 250 °C, control QD films showed a gradual decrease in the PLQY. Thermal energy facilitates interactions of the surface of QDs with ambient air, in contrast, QDs in the ZnS matrix did not show degradation at an annealing temperature of 200 °C. Eventually, QDs in the ZnS matrix exhibited a decrease of PLQY at an annealing temperature of 250 °C. A possible explanation for the degradation is the generation of permanent trap states due to the difference in the thermal expansion of the core and shell and thermally increased atomic mobility.[17,33]

We further investigated the effect of the ZnS matrix on the photostability of QDs by measuring PL intensity under continuous 375 nm laser excitation at 60 mW cm^{-2} (Figure 4d). QDs embedded in the ZnS matrix exhibited better photostability compared to oleic-acid-capped QD films, maintaining the initial PL intensity until 180 min. In contrast, control QD films showed a sharp decrease of less than 50% of the initial PL intensity within 20 min.

CONCLUSIONS

We report a strategy to encapsulate InP/ZnS QDs in an inorganic matrix by combining a biphasic ligand exchange method and a sol−gel method for the fabrication of inorganic films. We sought to replace native organic ligands of as-synthesized InP/ZnS QDs with the ZnS sol−gel precursor. The QDs were transferred to the ZnS solution via ligand exchange, forming a QD ink stabilized in the ZnS sol−gel solution. The development of QD inks can enable us to deposit QD films by various techniques such as spin-coating, slot-die-coating, blade-coating, spray-coating, and inkjet printing techniques. The ZnS matrix was formed by annealing the film cast by the QD ink, evidenced by XRD and PLE. We investigated the effect of the ZnS matrix on the optical properties and the stability of InP/ZnS QDs. The QDs in the ZnS matrix showed higher PLQY compared to control InP/ZnS films. We demonstrate stable QD solid films with a ZnS matrix; the materials retained their PLQYs after annealing at 200 °C for 1 h under ambient conditions, under continuous laser excitation at 60 mW cm^{-2}, and also after a month of storage under ambient conditions, representing a significant improvement in the existing materials.

ASSOCIATED CONTENT

Supporting Information

The Supporting Information is available free of charge at https://pubs.acs.org/doi/10.1021/acs.chemmater.0c02870.

^{1}H NMR spectra of oleic acid and oleic-acid-capped InP/ZnS QDs; histogram of QD size distribution; methods for the volume fraction measurements; thickness of QDs in the ZnS matrix; images of QDs in the ZnS matrix with and without a UV lamp; elemental mapping using energy-dispersive X-ray spectroscopy; excitation wavelength dependence of the PLQY; steady-state PL spectra of InP/ZnS QDs and InP/ZnS QDs; and fitting parameters of the PL decay (PDF)

https://dx.doi.org/10.1021/acs.chemmater.0c02870
Chem. Mater. XXXX, XXX, XXX−XXX

AUTHOR INFORMATION

Corresponding Author

Edward H. Sargent − *Department of Electrical and Computer Engineering, University of Toronto, Toronto, Ontario M5S 1A4, Canada;* orcid.org/0000-0003-0396-6495; Email: ted.sargent@utoronto.ca

Authors

Seungjin Lee − *Department of Electrical and Computer Engineering, University of Toronto, Toronto, Ontario M5S 1A4, Canada;* orcid.org/0000-0002-6318-0702

Laxmi Kishore Sagar − *Department of Electrical and Computer Engineering, University of Toronto, Toronto, Ontario M5S 1A4, Canada;* orcid.org/0000-0002-7656-7308

Xiyan Li − *Department of Electrical and Computer Engineering, University of Toronto, Toronto, Ontario M5S 1A4, Canada*

Yitong Dong − *Department of Electrical and Computer Engineering, University of Toronto, Toronto, Ontario M5S 1A4, Canada*

Bin Chen − *Department of Electrical and Computer Engineering, University of Toronto, Toronto, Ontario M5S 1A4, Canada*

Yuan Gao − *Department of Electrical and Computer Engineering, University of Toronto, Toronto, Ontario M5S 1A4, Canada;* orcid.org/0000-0001-9407-1528

Dongxin Ma − *Department of Electrical and Computer Engineering, University of Toronto, Toronto, Ontario M5S 1A4, Canada;* orcid.org/0000-0002-9790-5951

Larissa Levina − *Department of Electrical and Computer Engineering, University of Toronto, Toronto, Ontario M5S 1A4, Canada*

Aidan Grenville − *Department of Electrical and Computer Engineering, University of Toronto, Toronto, Ontario M5S 1A4, Canada*

Sjoerd Hoogland − *Department of Electrical and Computer Engineering, University of Toronto, Toronto, Ontario M5S 1A4, Canada;* orcid.org/0000-0002-3099-585X

F. Pelayo García de Arquer − *Department of Electrical and Computer Engineering, University of Toronto, Toronto, Ontario M5S 1A4, Canada;* orcid.org/0000-0003-2422-6234

Complete contact information is available at: https://pubs.acs.org/10.1021/acs.chemmater.0c02870

Author Contributions

†S.L. and L.K.S. contributed equally to this work.

Notes

The authors declare no competing financial interest.

ACKNOWLEDGMENTS

This work is supported by the Natural Sciences and Engineering Research Council of Canada (NSERC, grant number 537463-18). The authors acknowledge Huawei Canada for its financial support. This research was also supported by the National Research Foundation (NRF) of Korea (NRF-2020R1A6A3A03038131). We thank D. Kopilovic, E. Palmiano, L. Levina, and R. Wolowiec for the technical support.

REFERENCES

(1) Yin, Y.; Alivisatos, A. P. Colloidal nanocrystal synthesis and the organic−inorganic interface. *Nature* **2005**, *437*, 664−670.

(2) Pietryga, J. M.; Park, Y.-S.; Lim, J.; Fidler, A. F.; Bae, W. K.; Brovelli, S.; Klimov, V. I. Spectroscopic and Device Aspects of Nanocrystal Quantum Dots. *Chem. Rev.* **2016**, *116*, 10513−10622.

(3) Kippeny, T.; Swafford, L. A.; Rosenthal, S. J. Semiconductor Nanocrystals: A Powerful Visual Aid for Introducing the Particle in a Box. *J. Chem. Educ.* **2002**, *79*, 1094.

(4) Xu, G.; Zeng, S.; Zhang, B.; Swihart, M. T.; Yong, K.-T.; Prasad, P. N. New Generation Cadmium-Free Quantum Dots for Biophotonics and Nanomedicine. *Chem. Rev.* **2016**, *116*, 12234−12327.

(5) Reiss, P.; Carrière, M.; Lincheneau, C.; Vaure, L.; Tamang, S. Synthesis of Semiconductor Nanocrystals, Focusing on Nontoxic and Earth-Abundant Materials. *Chem. Rev.* **2016**, *116*, 10731−10819.

(6) Jang, E.; Kim, Y.; Won, Y.-H.; Jang, H.; Choi, S.-M. Environmentally Friendly InP-Based Quantum Dots for Efficient Wide Color Gamut Displays. *ACS Energy Lett.* **2020**, *5*, 1316−1327.

(7) Wu, Z.; Liu, P.; Zhang, W.; Wang, K.; Sun, X. W. Development of InP Quantum Dot-Based Light-Emitting Diodes. *ACS Energy Lett.* **2020**, *5*, 1095−1106.

(8) Healy, M. D.; Laibinis, P. E.; Stupik, P. D.; Barron, A. R. The reaction of indium(III) chloride with tris(trimethylsilyl)phosphine: a novel route to indium phosphide. *J. Chem. Soc., Chem. Commun.* **1989**, 359−360.

(9) Li, L.; Reiss, P. One-pot Synthesis of Highly Luminescent InP/ZnS Nanocrystals without Precursor Injection. *J. Am. Chem. Soc.* **2008**, *130*, 11588−11589.

(10) Kim, S.; Kim, T.; Kang, M.; Kwak, S. K.; Yoo, T. W.; Park, L. S.; Yang, I.; Hwang, S.; Lee, J. E.; Kim, S. K.; Kim, S.-W. Highly Luminescent InP/GaP/ZnS Nanocrystals and Their Application to White Light-Emitting Diodes. *J. Am. Chem. Soc.* **2012**, *134*, 3804−3809.

(11) Lim, J.; Bae, W. K.; Lee, D.; Nam, M. K.; Jung, J.; Lee, C.; Char, K.; Lee, S. InP@ZnSeS, Core@Composition Gradient Shell Quantum Dots with Enhanced Stability. *Chem. Mater.* **2011**, *23*, 4459−4463.

(12) Cao, F.; Wang, S.; Wang, F.; Wu, Q.; Zhao, D.; Yang, X. A. Layer-by-Layer Growth Strategy for Large-Size InP/ZnSe/ZnS Core−Shell Quantum Dots Enabling High-Efficiency Light-Emitting Diodes. *Chem. Mater.* **2018**, *30*, 8002−8007.

(13) Tessier, M. D.; Dupont, D.; De Nolf, K.; De Roo, J.; Hens, Z. Economic and Size-Tunable Synthesis of InP/ZnE (E = S, Se) Colloidal Quantum Dots. *Chem. Mater.* **2015**, *27*, 4893−4898.

(14) Won, Y.-H.; Cho, O.; Kim, T.; Chung, D.-Y.; Kim, T.; Chung, H.; Jang, H.; Lee, J.; Kim, D.; Jang, E. Highly efficient and stable InP/ZnSe/ZnS quantum dot light-emitting diodes. *Nature* **2019**, *575*, 634−638.

(15) Li, Y.; Hou, X.; Dai, X.; Yao, Z.; Lv, L.; Jin, Y.; Peng, X. Stoichiometry-Controlled InP-Based Quantum Dots: Synthesis, Photoluminescence, and Electroluminescence. *J. Am. Chem. Soc.* **2019**, *141*, 6448−6452.

(16) Zhang, H.; Hu, N.; Zeng, Z.; Lin, Q.; Zhang, F.; Tang, A.; Jia, Y.; Li, L. S.; Shen, H.; Teng, F.; Du, Z. High-Efficiency Green InP Quantum Dot-Based Electroluminescent Device Comprising Thick-Shell Quantum Dots. *Adv. Opt. Mater.* **2019**, *7*, No. 1801602.

(17) Moon, H.; Lee, C.; Lee, W.; Kim, J.; Chae, H. Stability of Quantum Dots, Quantum Dot Films, and Quantum Dot Light-Emitting Diodes for Display Applications. *Adv. Mater.* **2019**, *31*, No. 1804294.

(18) Ko, J.; Jeong, B. G.; Chang, J. H.; Joung, J. F.; Yoon, S.-Y.; Lee, D. C.; Park, S.; Huh, J.; Yang, H.; Bae, W. K.; Jang, S. G.; Bang, J. Chemically resistant and thermally stable quantum dots prepared by shell encapsulation with cross-linkable block copolymer ligands. *NPG Asia Mater.* **2020**, *12*, No. 19.

(19) Brown, R. P.; Gallagher, M. J.; Fairbrother, D. H.; Rosenzweig, Z. Synthesis and Degradation of Cadmium-Free InP and InPZn/ZnS Quantum Dots in Solution. *Langmuir* **2018**, *34*, 13924−13934.

(20) Nam, E.; Lee, C.; Kim, S. J.; Chung, H. K.; Chae, H. Stability and dispersion improvement of quantum-dot films by hydrosilylation between quantum-dot ligands and a siloxane matrix. *Opt. Express* **2019**, *27*, 20037−20046.

(21) Chen, S.; Cao, W.; Liu, T.; Tsang, S.-W.; Yang, Y.; Yan, X.; Qian, L. On the degradation mechanisms of quantum-dot light-emitting diodes. *Nat. Commun.* **2019**, *10*, No. 765.
(22) van Sark, W. G. J. H. M.; Frederix, P. L. T. M.; Bol, A. A.; Gerritsen, H. C.; Meijerink, A. Blueing, Bleaching, and Blinking of Single CdSe/ZnS Quantum Dots. *ChemPhysChem* **2002**, *3*, 871−879.
(23) Pechstedt, K.; Whittle, T.; Baumberg, J.; Melvin, T. Photoluminescence of Colloidal CdSe/ZnS Quantum Dots: The Critical Effect of Water Molecules. *J. Phys. Chem. C* **2010**, *114*, 12069−12077.
(24) Gao, L.; Quan, L. N.; García de Arquer, F. P.; Zhao, Y.; Munir, R.; Proppe, A.; Quintero-Bermudez, R.; Zou, C.; Yang, Z.; Saidaminov, M. I.; Voznyy, O.; Kinge, S.; Lu, Z.; Kelley, S. O.; Amassian, A.; Tang, J.; Sargent, E. H. Efficient near-infrared light-emitting diodes based on quantum dots in layered perovskite. *Nat. Photonics* **2020**, *14*, 227−233.
(25) Masi, S.; Gualdrón-Reyes, A. F.; Mora-Seró, I. Stabilization of Black Perovskite Phase in $FAPbI_3$ and $CsPbI_3$. *ACS Energy Lett.* **2020**, *5*, 1974−1985.
(26) Ramasamy, P.; Ko, K.-J.; Kang, J.-W.; Lee, J.-S. Two-Step "Seed-Mediated" Synthetic Approach to Colloidal Indium Phosphide Quantum Dots with High-Purity Photo- and Electroluminescence. *Chem. Mater.* **2018**, *30*, 3643−3647.
(27) Hens, Z.; Martins, J. C. A Solution NMR Toolbox for Characterizing the Surface Chemistry of Colloidal Nanocrystals. *Chem. Mater.* **2013**, *25*, 1211−1221.
(28) Hughes, K. E.; Stein, J. L.; Friedfeld, M. R.; Cossairt, B. M.; Gamelin, D. R. Effects of Surface Chemistry on the Photophysics of Colloidal InP Nanocrystals. *ACS Nano* **2019**, *13*, 14198−14207.
(29) Tavasoli, E.; Guo, Y.; Kunal, P.; Grajeda, J.; Gerber, A.; Vela, J. Surface Doping Quantum Dots with Chemically Active Native Ligands: Controlling Valence without Ligand Exchange. *Chem. Mater.* **2012**, *24*, 4231−4241.
(30) Fafarman, A. T.; Koh, W.-k.; Diroll, B. T.; Kim, D. K.; Ko, D.-K.; Oh, S. J.; Ye, X.; Doan-Nguyen, V.; Crump, M. R.; Reifsnyder, D. C.; Murray, C. B.; Kagan, C. R. Thiocyanate-Capped Nanocrystal Colloids: Vibrational Reporter of Surface Chemistry and Solution-Based Route to Enhanced Coupling in Nanocrystal Solids. *J. Am. Chem. Soc.* **2011**, *133*, 15753−15761.
(31) Kuo, T.-R.; Hung, S.-T.; Lin, Y.-T.; Chou, T.-L.; Kuo, M.-C.; Kuo, Y.-P.; Chen, C.-C. Green Synthesis of InP/ZnS Core/Shell Quantum Dots for Application in Heavy-Metal-Free Light-Emitting Diodes. *Nanoscale Res. Lett.* **2017**, *12*, No. 537.
(32) Shen, W.; Tang, H.; Yang, X.; Cao, Z.; Cheng, T.; Wang, X.; Tan, Z.; You, J.; Deng, Z. Synthesis of highly fluorescent InP/ZnS small-core/thick-shell tetrahedral-shaped quantum dots for blue light-emitting diodes. *J. Mater. Chem. C* **2017**, *5*, 8243−8249.
(33) Rowland, C. E.; Liu, W.; Hannah, D. C.; Chan, M. K. Y.; Talapin, D. V.; Schaller, R. D. Thermal Stability of Colloidal InP Nanocrystals: Small Inorganic Ligands Boost High-Temperature Photoluminescence. *ACS Nano* **2014**, *8*, 977−985.

https://dx.doi.org/10.1021/acs.chemmater.0c02870
Chem. Mater. XXXX, XXX, XXX−XXX